



Letter

The critical pressure for driving a red blood cell through a contracting microfluidic channel

Tenghu Wu^a, Quan Guo^b, Hongshen Ma^b, James J. Feng^{a,c,*}^a Department of Chemical and Biological Engineering, University of British Columbia, Vancouver, BC V6T 1Z3, Canada^b Department of Mechanical Engineering, University of British Columbia, Vancouver, BC V6T 1Z4, Canada^c Department of Mathematics, University of British Columbia, Vancouver, BC V6T 1Z2, Canada

ARTICLE INFO

Article history:

Received 5 September 2015

Accepted 14 November 2015

Available online 28 November 2015

*This article belongs to the Biomechanics and Interdiscipline

Keywords:

Cell deformation

Erythrocyte deformability

Membrane modulus

Membrane rigidification

Capillary occlusion

ABSTRACT

When a red blood cell (RBC) is driven by a pressure gradient through a microfluidic channel, its passage or blockage provides a measure of the rigidity of the cell. This has been developed as a means to separate RBCs according to their mechanical properties, which are known to change with pathological conditions such as malaria infection. In this study, we use numerical simulations to establish a quantitative connection between the minimum pressure needed to drive an RBC through a contracting microfluidic channel and the rigidity of the cell membrane. This provides the basis for designing such devices and interpreting the experimental data.

© 2015 The Authors. Published by Elsevier Ltd on behalf of The Chinese Society of Theoretical and Applied Mechanics. This is an open access article under the CC BY-NC-ND license (<http://creativecommons.org/licenses/by-nc-nd/4.0/>).

Red blood cells (RBCs) are extremely flexible. This allows the RBCs to pass through microcapillaries of size much smaller than theirs. When infected by the malaria parasite *Plasmodium falciparum*, the RBC gradually loses its deformability, which leads to blockage of the blood circulation in microcapillaries. As models for this process, microfluidic assays have been designed in which the critical pressure required to push red cells through a contraction is used as a measure of the cell's deformability [1,2]. Similar devices have been used to separate cells according to their size and rigidity [3]. Since RBCs are known to rigidify under pathological conditions such as malaria infection [4], microfluidic channels also hold promise as a diagnostic and fractionation tool [5]. Compared with alternative methods to measure mechanical properties of RBCs, such as cell stretching by optical tweezers [6] and micropipette aspiration [7], the microfluidic channel has the advantage of closely mimicking the flow geometry *in vivo*.

Ma and coworkers [2,3] have designed a “microfluidic funnel ratchet,” which consists of a series of contractions followed by sudden expansions (Fig. 1). In such a device, the critical pressure drop for pushing the cell through the channel depends on the

deformability of the cell. The more flexible the cell, the less pressure needed. However, no quantitative correlation exists that relates the measured critical pressure drop to the shear and bending moduli of the cell. Ma et al. [2,3] employed the Young–Laplace equation to estimate the cell's cortical tension from the measured critical pressure drop. In this model, the cell was treated as a liquid drop with a constant cortical tension T_c , which was related to the critical pressure drop ΔP_c through

$$\Delta P_c = T_c \left(\frac{1}{R_a} - \frac{1}{R_b} \right), \quad (1)$$

where R_a and R_b are the radii of curvature at the cell's front and back. However, the cell membrane is elastic and differs considerably from a fluid interface. For example, the in-plane tension will likely vary along the membrane according to the local strain. Besides, the bending rigidity of the membrane may also play a role.

To address these issues, we carry out numerical simulations using a more realistic representation of the mechanical properties of the cell, with an elastic membrane enclosing a viscous cytosol. The physical model and numerical method are based on the recent study of Wu and Feng [8]. The cell membrane is represented by a discrete particle–spring network (Fig. 2(a)), with elasticity against in-plane strain and bending (Fig. 2(b)). The fluids inside and outside of the membrane are discretized by particles as well (Fig. 2(c)), using the framework of smoothed particle hydrodynamics [9]. We

* Corresponding author at: Department of Chemical and Biological Engineering, University of British Columbia, Vancouver, BC V6T 1Z3, Canada.

E-mail address: jfeng@chbe.ubc.ca (J.J. Feng).

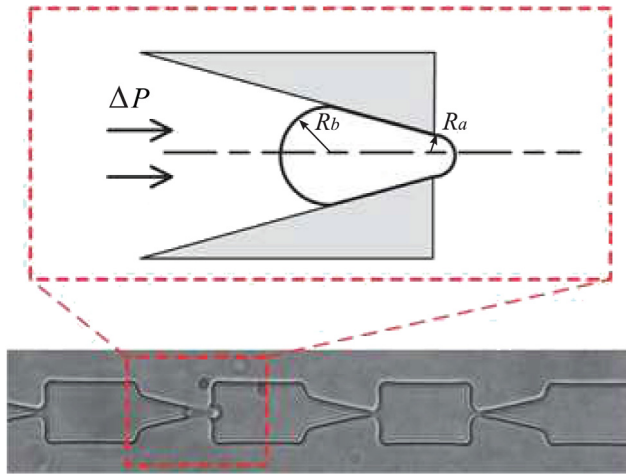


Fig. 1. The geometry of the microfluidic device studied by Ma et al. [2,3]. Source: Adapted from Ref. [2] with permission © Royal Society of Chemistry.

use linear springs of an elastic coefficient k_s such that the elastic energy for in-plane deformation is

$$E_s = \sum_{i,j} \frac{k_s}{2} (L_{ij} - L_{ij,0})^2, \quad (2)$$

where the summation is over all pairs of adjacent vertices i and j , L_{ij} is the length of the spring connecting them, and $L_{ij,0}$ is its resting length. In addition, we adopt the following bending energy [10]:

$$E_b = \sum_{i,j} 2k_b \tan^2 \left(\frac{\theta_{ij}}{2} \right), \quad (3)$$

where k_b is the bending modulus and the summation is over all pairs of neighboring triangles i and j and θ_{ij} is the angle between their normals. Note that this bending energy assumes zero spontaneous curvature for the membrane.

The red cells are known to conserve their surface area. In our particle model, this is implemented through an energy penalty

against local area dilatation:

$$E_A = \frac{k_d}{2} \sum_{j=1}^N \left(\frac{A_0^j - A^j}{A_0^j} \right)^2 A_0^j, \quad (4)$$

where k_d is a constant, A_0^j is the undeformed area of the j th triangle, and the summation is over all N triangles of the RBC membrane. Finally, we include an energy penalty against the change of the total cell volume:

$$E_V = \frac{k_v}{2} V_0 \left(\frac{V_0 - V}{V_0} \right)^2, \quad (5)$$

where k_v is a constant coefficient, and V_0 is the initial volume of the cell. Under large forcing and severe cell deformation, this volume constraint helps to prevent fluid particles from penetrating the membrane. Using Eqs. (2)–(5), we write the total elastic energy of the cell membrane as $E_m = E_s + E_b + E_A + E_V$. The elastic force acting on each membrane particle can then be calculated as

$$\mathbf{f}_m = -\partial E_m / \partial \mathbf{r}, \quad (6)$$

\mathbf{r} being the position of the membrane particle.

The fluid motion is solved by using the smoothed particle hydrodynamics (SPH) method [9]. For the membrane particles, the elastic force \mathbf{f}_m is added to the hydrodynamic force on the right-hand side of the momentum equation. We have tested convergence of the results with respect to spatial resolution. For an initial particle spacing $d \leq 0.15R_0$, R_0 being the radius of the undeformed RBC, the numerical results no longer depend on d . Thus, the simulations have been carried out using $d = 0.15R_0$.

The surface of the undeformed red cell is obtained from the formula of Evans and Fung [11]:

$$D(r) = \sqrt{1 - (r/R_0)^2} [C_0 + C_1(r/R_0)^2 + C_2(r/R_0)^4], \quad (7)$$

where $D(r)$ is the thickness of the RBC as a function of distance from the center, and R_0 is the RBC's radius. In our simulation, we set $(R_0, C_0, C_1, C_2) = (3.9, 0.81, 7.83, -4.39) \mu\text{m}$ [12]. With these parameters, the red cell's volume and surface area are about $92 \mu\text{m}^3$ and $132 \mu\text{m}^2$, respectively, in agreement with experimental values [13,14]. The triangular mesh on the cell surface was automatically created by the commercial software GAMBIT. Once this

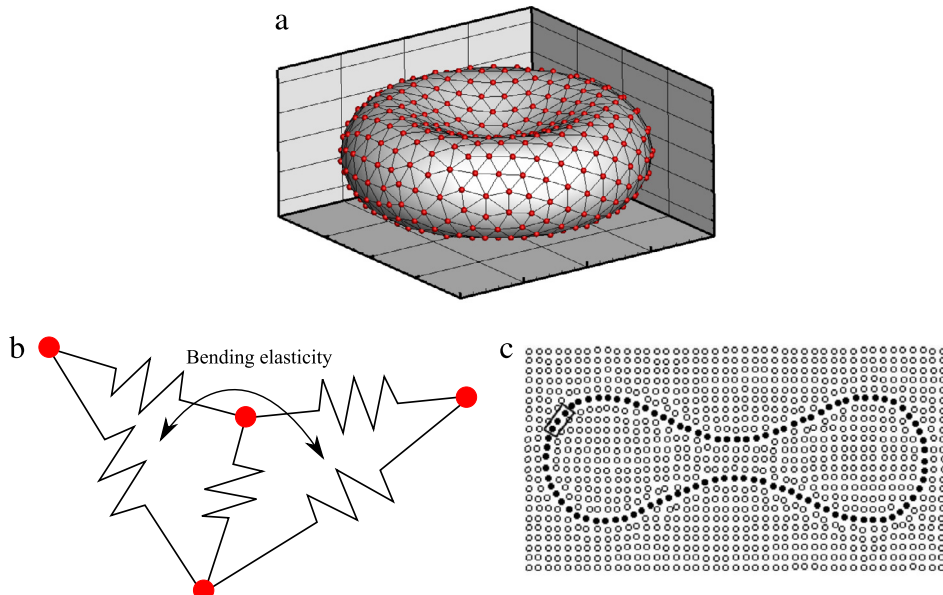


Fig. 2. (a) The RBC membrane is modeled by a triangular particle–spring meshwork. (b) Each segment is an elastic spring (Eq. (2)), and there is bending elasticity between neighboring triangles (Eq. (3)). (c) The interior and exterior fluids are discretized by particles, whose movement approximates the Navier–Stokes equation in the smoothed-particle-hydrodynamics framework [9].

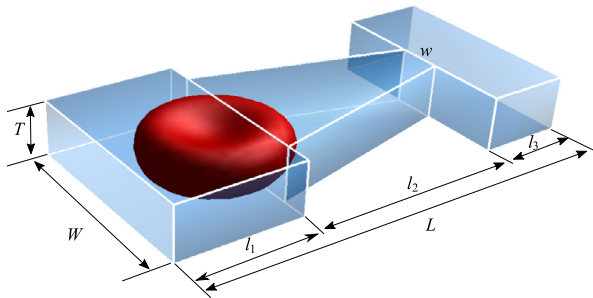


Fig. 3. Schematic of the computational domain.

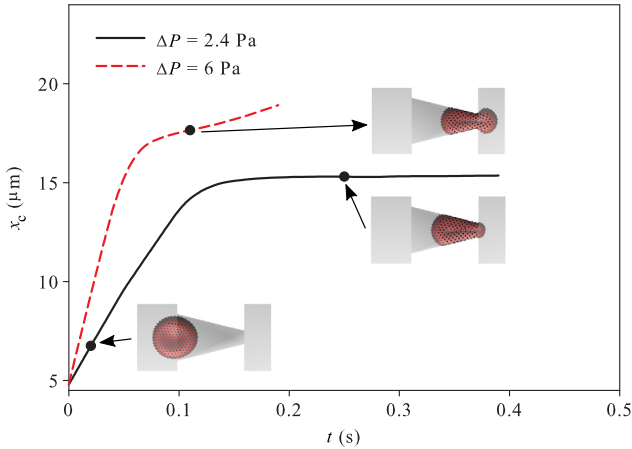


Fig. 4. Trajectories of the RBC center of mass through a contraction with $T = 3 \mu\text{m}$ and $w = 2.4 \mu\text{m}$ at two pressure drops.

initial mesh is created, the edge lengths are taken to be the resting length $L_{ij,0}$ of the springs so that the initial in-plane energy is $E_s = 0$ (cf. Eq. (2)). The shear modulus G_s and bending modulus κ of the cell membrane can be related to the coefficients of our mechanical model through [15,16]: $G_s = \frac{\sqrt{3}}{4} k_s$ and $\kappa = \frac{1}{2\sqrt{3}} k_b$.

The computational domain is shown in Fig. 3. The geometry of the microfluidic channel is inspired by experimental setups of Ma and coworkers [2,3], as shown in Fig. 1. The entrance has a rectangular cross section of width W and thickness T . The same thickness is maintained throughout the entire conduit, but the width contracts through a 14° slope to a narrower width w . Further downstream is a sudden expansion to a cross-section that is identical to the one at the entrance. In the simulations, we have kept the segmental lengths constant: $l_1 = 7.6 \mu\text{m}$, $l_2 = 12 \mu\text{m}$, $l_3 = 4.4 \mu\text{m}$, and tested a range of T (3–3.6 μm) and w (1.8–3 μm) values to vary the degree of blockage. When w changes, we vary W according to $W = w + 9.6 \mu\text{m}$ so that the shoulders upstream and downstream of the contraction maintain constant widths. The shear and bending moduli of the RBC are chosen according to experimental measurements [7,17]: $G_s = 5 \text{ N}/\mu\text{m}$ and $\kappa = 2 \times 10^{-19} \text{ J}$.

Figure 4 shows the trajectories of the cell's center of mass x_c at two pressure drops. The RBC passes through the contraction at the higher $\Delta P = 6 \text{ Pa}$ but not the lower $\Delta P = 2.4 \text{ Pa}$. For the lower ΔP , the RBC is eventually stuck in the contraction, with a small tongue extending downstream. Two snapshots of the RBC inside the domain are shown at $t = 0.02 \text{ s}$ and 0.25 s . Note that the model does not account for solid-solid friction between the membrane and the wall. However, a short-range repulsion force is assumed between the membrane and wall particles when their separation falls below a threshold, which is set to be the initial particle spacing d . This repulsion prevents the membrane particles from penetrating the channel walls, but does not affect the result

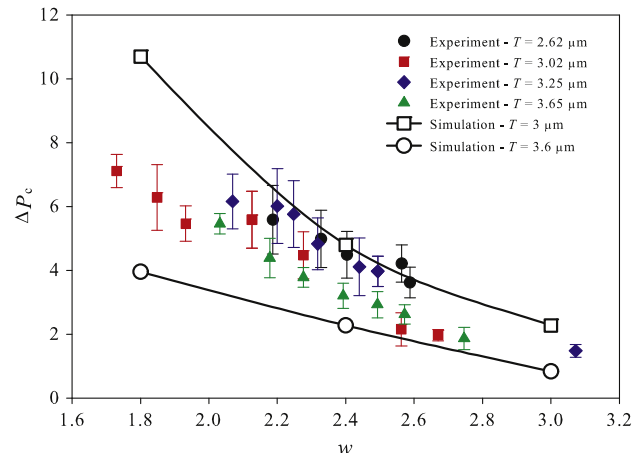


Fig. 5. The critical pressure drop ΔP_c required to push the RBC through funnel channels depends on the dimensions of the narrowest part of the channel, its thickness T and width w . Experimental data over a comparable range of dimensions are also shown for comparison.

otherwise. The occlusion is due to the inability of the RBC to deform sufficiently, against in-plane and bending elasticity, so as to pass through the narrowest part. For the higher pressure drop $\Delta P = 6 \text{ Pa}$, the red cell does deform sufficiently to pass through the contraction. A snapshot is shown at $t = 0.11 \text{ s}$ that illustrates the passage. We have tested the pressure drop ΔP from 1.2 Pa to 6 Pa and determined a critical pressure drop $\Delta P_c = 4.56 \text{ Pa}$ for the geometry of Fig. 4. Only pressure drops higher than this can push the RBC through the channel. At lower ΔP , the cell blocks the channel.

In Fig. 5, we investigate how the critical pressure ΔP_c varies with the dimensions of the narrowest opening, with thickness T and width w . As expected, the model predicts the critical pressure to decrease with increasing w or T . For the smaller $T = 3 \mu\text{m}$, the decreasing trend of ΔP_c with increasing w is stronger, by more than a factor of 4 as w increases from $1.8 \mu\text{m}$ to $3 \mu\text{m}$. The trend is milder for the larger $T = 3.6 \mu\text{m}$. Besides, we also expect ΔP_c to rise sharply as w shrinks; this is evident for the $T = 3 \mu\text{m}$ curve already.

In Fig. 5, we have also included experimental data measured in channels with different sizes of the narrowest part, with thickness T ranging from $2.62 \mu\text{m}$ to $3.65 \mu\text{m}$ and width w from $1.7 \mu\text{m}$ to $3.07 \mu\text{m}$. The ΔP_c data bear out the decreasing trend with w , and generally fall between the two computed curves, although the two T values used in the computation do not bracket the experimental T values perfectly. In light of this, the quantitative agreement may be considered reasonably good. We can speculate on the causes for the discrepancies. For one, we have assumed simple constitutive equations for the membrane elasticity Eqs. (2) and (3). In reality, the red cell membrane exhibits complex viscoelastic rheology [18]. Furthermore, we have used fixed values for the shear modulus G_s and the bending modulus κ , whereas normal red cells exhibit considerable variability [5,19]. Finally, careful inspection of the experimental data shows that some data points for taller channels (i.e., larger T) seem to fall above those for channels of smaller T . Thus, experimental errors, e.g. due to solid contact and friction between the cell and channel wall, fluid leakage for taller channels, and inaccuracies in measuring the pore dimensions T and w , may have contributed to the discrepancies as well.

In summary, we have employed a discrete particle-based model to simulate the passage of RBC through a funnel-shape microfluidic channel. The simulation results agree well with existing experimental data, and provide a quantitative correlation between the measurable critical pressure drop ΔP_c and the deformability of the cell. This work suggests the feasibility of using microfluidic essays

for measuring cell deformation and separating cells according to their rigidity, potentially providing a diagnostic for diseases such as malaria. For this purpose, of course, larger-scale computations need to be carried out to build a database covering wider ranges of geometric parameters as well as mechanical parameters that correspond to healthy and diseased cells.

Acknowledgments

The study was supported by the Natural Sciences and Engineering Research Council of Canada (NSERC 05862 and 06541) and the Canada Research Chair program. JJF acknowledges additional support by the Peter Wall Institute for Advanced Studies during his tenure as Wall Scholar. TW acknowledges partial support by the Chinese Government Award for Outstanding Self-Financed Students Abroad. HM acknowledges funding from the Canadian Institutes of Health Research (CIHR 259107, 325373, 322375) and the Canadian Blood Services (CIHR-BUC21403-HM). QG acknowledges funding from the UBC Four Year Doctoral Fellowship.

References

- [1] J.P. Shelby, J. White, K. Ganesan, et al., A microfluidic model for single-cell capillary obstruction by *Plasmodium falciparum*-infected erythrocytes, *Proc. Natl. Acad. Sci. USA* 100 (2003) 14618–14622.
- [2] Q. Guo, S.J. Reiling, P. Rohrbach, et al., Microfluidic biomechanical assay for red blood cells parasitized by *Plasmodium falciparum*, *Lab Chip* 12 (2012) 1143–1150.
- [3] S.M. McFaul, B.K. Lin, H. Ma, Cell separation based on size and deformability using microfluidic funnel ratchets, *Lab Chip* 12 (2012) 2369–2376.
- [4] C.A. Moxon, G.E. Grau, A.G. Craig, Malaria: modification of the red blood cell and consequences in the human host, *Br. J. Haematol.* 154 (2011) 670–679.
- [5] Q. Guo, S.P. Duffy, K. Matthews, et al., Microfluidic analysis of red blood cell deformability, *J. Biomech.* 47 (2014) 1767–1776.
- [6] M. Dao, C.T. Lim, S. Suresh, Mechanics of the human red blood cell deformed by optical tweezers, *J. Mech. Phys. Solids* 51 (2003) 2259–2280.
- [7] G.B. Nash, E. O'Brien, E.C. Gordon-Smith, et al., Abnormalities in the mechanical properties of red blood cells caused by *Plasmodium falciparum*, *Blood* 74 (1989) 855–861.
- [8] T. Wu, J.J. Feng, Simulation of malaria-infected red blood cells in microfluidic channels: Passage and blockage, *Biomicrofluidics* 7 (2013) 044115.
- [9] J.J. Monaghan, Smoothed particle hydrodynamics, *Rep. Progr. Phys.* 68 (2005) 1703–1759.
- [10] S. Wada, R. Kobayashi, Numerical simulation of various shape changes of a swollen red blood cell by decrease of its volume, *Trans. Japan Soc. Mech. Eng.* 69 (2003) 14–21.
- [11] E. Evans, Y. Fung, Improved measurements of the erythrocyte geometry, *Microvasc. Res.* 4 (1972) 335–347.
- [12] S.M. Hosseini, J.J. Feng, A particle-based model for the transport of erythrocytes in capillaries, *Chem. Eng. Sci.* 64 (2009) 4488–4497.
- [13] A. Esposito, J. Chojniet, J. Skepper, et al., Quantitative imaging of human red blood cells infected with *Plasmodium falciparum*, *Biophys. J.* 99 (2010) 953–960.
- [14] Y.M. Serebrennikova, J. Patel, W.K. Milhous, et al., Quantitative analysis of morphological alterations in *Plasmodium falciparum* infected red blood cells through theoretical interpretation of spectral measurements, *J. Theoret. Biol.* 265 (2010) 493–500.
- [15] T. Omori, T. Ishikawa, D. Barthes-Biesel, et al., Comparison between spring network models and continuum constitutive laws: Application to the large deformation of a capsule in shear flow, *Phys. Rev. E* 83 (2011) 041918.
- [16] D.H. Boal, M. Rao, Topology changes in fluid membranes, *Phys. Rev. A* 46 (1992) 3037–3045.
- [17] E. Evans, New membrane concept applied to the analysis of fluid shear- and micropipette-deformed red blood cells, *Biophys. J.* 13 (1973) 941–954.
- [18] D.A. Fedosov, B. Caswell, G.E. Karniadakis, A multiscale red blood cell model with accurate mechanics, rheology, and dynamics, *Biophys. J.* 98 (2010) 2215–2225.
- [19] R.M. Hochmuth, R.E. Waugh, Erythrocyte membrane elasticity and viscosity, *Annu. Rev. Physiol.* 49 (1987) 209–219.